Enhanced spin-orbit torque by engineering Pt resistivity in Pt/Co/AlO_x structures

Jae Wook Lee,[1] Young-Wan Oh,[1] Seung-Young Park,[2] Adriana I. Figueroa,[3] Gerrit van der Laan,[3] Gyungchoon Go,[4] Kyung-Jin Lee,[4,5] and Byong-Guk Park[1,*]

[1]*Department of Materials Science and Engineering, KAIST, Daejeon 34141, Korea*
[2]*Spin Engineering Physics Team, Division of Scientific Instrument, KBSI, Daejeon 34133, Korea*
[3]*Magnetic Spectroscopy Group, Diamond Light Source, Didcot OX11 0DE, United Kingdom*
[4]*Department of Materials Science and Engineering, Korea University, Seoul 02841, Korea*
[5]*KU-KIST Graduate School of Converging Science and Technology, Korea University, Seoul 02841, Korea*

(Received 11 November 2016; revised manuscript received 13 June 2017; published 3 August 2017)

The magnetization direction in heavy-metal (HM)/ferromagnet bilayers can be electrically controlled by spin-orbit torque (SOT); however, the efficiency of the SOT which depends on the spin-orbit coupling of the HM layer or its spin-Hall angle has to be improved further for actual applications. In this study, we report a significant enhancement of the spin-Hall effect of Pt and resultant SOT in Pt/Co/AlO_x structures by controlling the Pt resistivity. We observed that the effective spin-Hall angle increases about three times as the resistivity of Pt layer is increased 1.6 times by changing the Ar deposition pressure from 3 to 50 mTorr. This enhancement in effective spin-Hall angle is confirmed by the reduction in the critical current for SOT-induced magnetization switching. Furthermore, x-ray absorption spectroscopy analysis reveals a non-negligible contribution of the interfacial spin-orbit coupling to the effective spin-Hall angle. Our result, the efficient control of effective spin Hall angle by controlling the HM resistivity, paves the way to improved switching efficiency in SOT-active devices.

DOI: 10.1103/PhysRevB.96.064405

I. INTRODUCTION

Spintronic devices have attracted considerable attention as viable alternatives to their traditional electronic counterparts as they offer nonvolatile memory and logic applications [1,2]. For a wider application of spintronic devices, it is essential to find an efficient way to switch the magnetization. In this respect, the discovery of spin-orbit torque (SOT) in heavy-metal (HM)/ferromagnet (FM) bilayer structures [3,4] is of considerable interest. In the case of conventional spin-transfer torque [5], a ferromagnetic polarizer supplies a spin-polarized current and therefore the ratio of spin to charge current, i.e., the spin polarization, cannot exceed 1. In sharp contrast, in the case of SOT, the spin-angular momentum is supplied from the lattice through spin-orbit coupling and thus there is no limit for the spin polarization (or effective spin-Hall angle). Recent studies [6,7] have found exceptional properties of spin-Hall angles larger than 1 and huge SOT in novel materials such as topological insulators. Despite their large spin-Hall angle, a practical use of these materials is yet premature. As a result, much effort has been devoted to finding HM materials with a large spin-Hall angle [8–17].

In order to efficiently engineer materials with large spin-Hall angles, it is important to address the so-far unanswered question concerning the microscopic origin of the SOT. One of these questions is the relation between the resistivity of the HM layer and the spin-Hall angle. The importance of this question is threefold. First, experiments have found that spin-Hall angles of 5*d* elements are 0.07–0.1 for Pt [8,9], –(0.12–0.15) for β-Ta [4], and –0.33 for β-W [10]. An interesting observation is that HMs exhibiting a larger spin-Hall angle show a higher resistivity ρ, i.e., $\rho(\beta\text{-W}) > \rho(\beta\text{-Ta}) > \rho(\text{Pt})$. A possible interpretation is the intrinsic spin-Hall effect of bulk HM [18,19] as the intrinsic mechanism is irrelevant with the electron scattering, and the spin-Hall angle for this mechanism is therefore proportional to the resistivity. However, it is not easy to unravel the role of the HM resistivity in SOT (or spin-Hall angle) by comparing these different HM elements since not only the resistivity but also the spin-orbit coupling and the number of *d* electrons vary. Second, a more conductive HM is preferred for applications to curtail joule heating and power consumption. In this respect, Pt is an attractive candidate but for practical applications its spin-Hall angle should be further increased. Third, a recent theoretical study by Wang *et al.* [20] predicted a larger spin-Hall angle for a more resistive Pt. This theory also emphasized a dominant contribution from the FM/HM interface to the spin-Hall effect rather than a contribution from the bulk part of HM. However, this prediction has not yet been tested experimentally.

In this paper, we experimentally investigate the relationship between the resistivity and the spin-Hall angle of Pt. We find a significant enhancement of the spin-Hall effect of Pt and resultant SOT in Pt/Co/AlO_x structures by modulating the Pt resistivity. By changing the Ar deposition pressure from 3 to 50 mTorr, the resistivity of the Pt layer increases by a factor of 1.6, which in turn gives an enhancement in the spin-Hall angle of about three times. The enhancement of the SOT for samples with a more resistive Pt layer is confirmed by SOT-induced magnetization switching experiments, where the switching current gradually diminishes for samples grown in higher Ar pressures. Furthermore, x-ray absorption spectroscopy (XAS) and x-ray magnetic circular dichroism (XMCD) measurements reveal a sizable contribution of the interfacial spin-orbit coupling to the SOT. Our result, the efficient control of the effective spin-Hall angle and hence of SOT by controlling the HM resistivity, opens up a novel way to improve the switching efficiency in SOT-active devices.

*Corresponding author: bgpark@kaist.ac.kr

II. EXPERIMENTAL

Samples of Pt(5 nm)/Co(0.8 nm)/AlO_x(1.8 nm) structure with Ta(3 nm) underlayer were deposited at room temperature on thermally oxidized silicon wafers using magnetron sputtering with a base pressure $<3.0 \times 10^{-8}$ Torr. The Pt layers were grown under various Ar pressures ranging from 3 to 50 mTorr in order to modulate the resistivity. The AlO_x layer on top was formed by depositing a metallic Al layer, which was then exposed to oxygen plasma. After deposition, the samples were patterned into a Hall bar structure with a 5 μm $\times$ 5 μm cross using photolithography and ion-milling technique. Finally, a Ru layer (50 nm) was used as a contact pad for transport measurements. Magnetic properties of the unpatterned samples were measured using a vibrating sample magnetometer (VSM). The SOT analysis was done using the harmonic anomalous Hall measurement technique [21–23], where the first and second harmonic Hall voltages generated by an ac current with a frequency ω(=50 Hz) were simultaneously measured as a function of the in-plane magnetic field.

The SOT-induced switching experiments were performed by sweeping a pulsed current of 50 μs under an in-plane field of 10 mT along the current direction, which is required for deterministic switching [3,24,25]. We note that the applied in-plane magnetic field for both harmonic Hall and magnetization switching measurements has a slight out-of-plane tilt angle (1–4°) from the film plane to prevent multidomain formation. XAS and XMCD measurements were carried out using the high-field magnet on beamline I10 at the Diamond Light Source, UK. The degree of circular polarization across the Co $L_{2,3}$ edges was ~100% and the XAS signal was recorded using total-electron-yield detection at room temperature. The XMCD signal was obtained by taking the difference between the XAS spectra measured with opposite helicities of the x rays at a fixed magnetic field. A magnetic field of 8 T was applied along the x-ray beam direction, which is normal to the sample surface.

III. RESULTS AND DISCUSSION

We first endeavored to control the Pt resistivity by regulating the Ar pressure during Pt deposition. The resistivity is expected to be higher for a Pt layer grown under higher pressure since the reduced kinetic energy of sputtered atoms leads to imperfections in the crystal structure [26]. In order to properly compare the resistance of the different Pt layers grown under nonidentical conditions, it is important to preserve a uniform Pt layer thickness across all samples. The thickness of the Pt layers deposited under various Ar pressures was verified using x-ray reflectivity (XRR) analysis as shown in Fig. 1(a). The identical periodicity of the XRR oscillations confirms that all samples have the same Pt layer thickness. The thickness, density, and roughness of the Pt layers obtained from the XRR analysis are listed in Table I. The roughness shows a slightly increasing trend with Ar pressure while the thickness and density remain nearly constant over all samples. After the thickness calibration by XRR, the resistivity of the Pt layer for each Pt/Co/AlO_x sample was measured. The results are shown as a function of Ar pressure in Fig. 1(b). The Pt resistivity increases linearly with Ar pressure and reaches

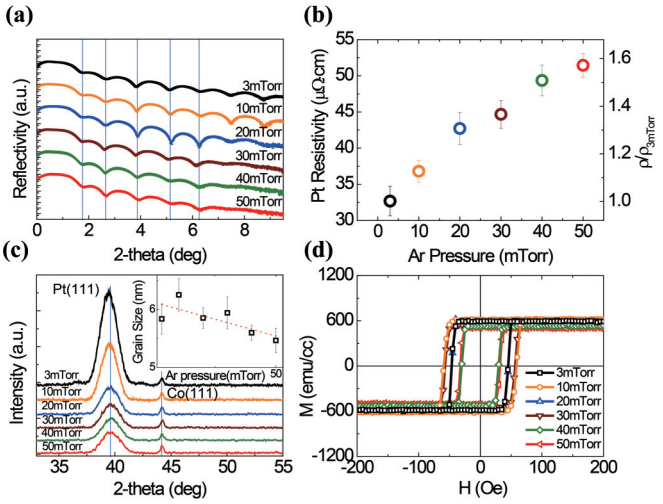

FIG. 1. Dependence of various properties of the samples grown under different Ar pressure during Pt deposition. (a) X-ray reflectivity data for Ta (3 nm)/Pt (5 nm) bilayer samples. (b) Pt layer resistivity as a function of a deposition pressure. (c) X-ray diffraction spectra for Pt/Co/AlO_x stacks. (d) Perpendicular magnetization hysteresis loops obtained using VSM for Pt/Co/AlO_x stacks.

a value of almost 1.6 times higher for Pt deposited under 50 mTorr, compared to 3 mTorr. Figure 1(c) shows the x-ray diffraction patterns demonstrating a lower crystallinity and smaller grain size (inset) for Pt layers grown under higher Ar pressure. This low crystallinity and small grain size induce additional scattering that might be responsible for the increased resistivity. We note that the perpendicular magnetic anisotropy is achieved for all samples and the saturation magnetization M_s is not significantly affected by the change in deposition pressure, as seen in Fig. 1(d), from the loops obtained by VSM.

We next investigated the dependence of the SOT on the Pt resistivity using a harmonic lock-in technique [21–23] as schematically illustrated in Fig. 2(a). Figures 2(b), 2(c), and 2(d) show the first ($V_{1\omega}$) and second ($V_{2\omega}$) harmonic Hall voltages of the samples with Pt layers grown at 3, 20, and 50 mTorr, respectively, as a function of the in-plane external field. $V_{1\omega}$, representing the perpendicular component of the magnetization, decreases with increasing in-plane magnetic field, which demonstrates the rotation of the magnetization

TABLE I. Thickness, density, and roughness data obtained from the XRR analysis for Pt layers deposited under various deposition pressures.

Pt deposition pressure (mTorr)	Thickness (nm)	Density (g/cm^3)	Roughness (nm)
3	5.04	19.64	0.28
10	5.04	19.82	0.34
20	4.90	20.47	0.44
30	5.05	19.63	0.55
40	5.00	19.61	0.57
50	4.96	19.42	0.59

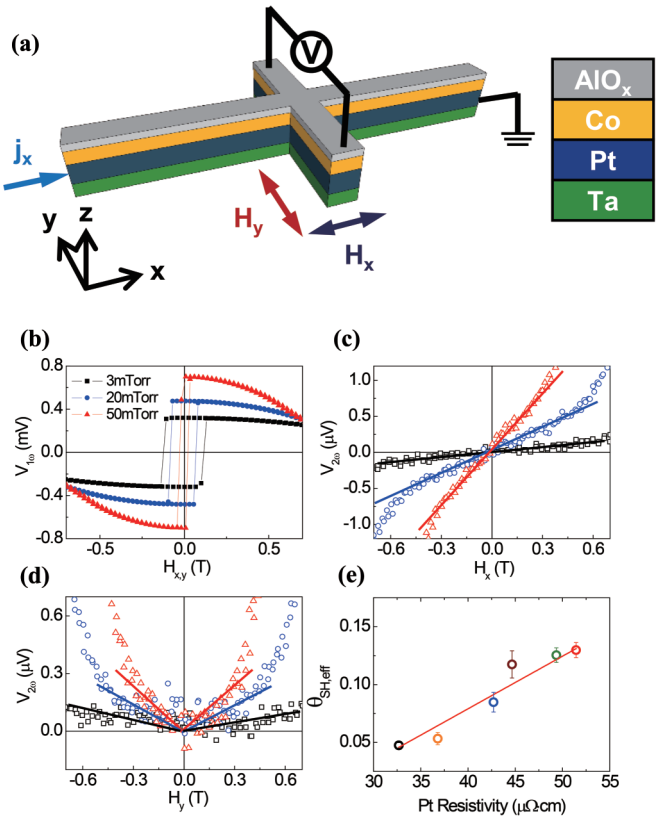

FIG. 2. Dependence of the SOT on the Pt resistance obtained by harmonic anomalous Hall measurements. (a) Schematic experimental setup for SOT measurements. (b) First harmonic Hall voltage $V_{1\omega}$. (c),(d) Second harmonic signals $V_{2\omega}$ with an ac current j_x of 2 mA along the x axis for the Pt/Co/AlO_x stacks as a function of in-plane magnetic field, H_x (c) and H_y (d). Lines in (c) and (d) are linear fitting lines, which correspond to the first derivative of $V_{2\omega}$. (e) Extracted effective spin-Hall angle vs Pt resistivity.

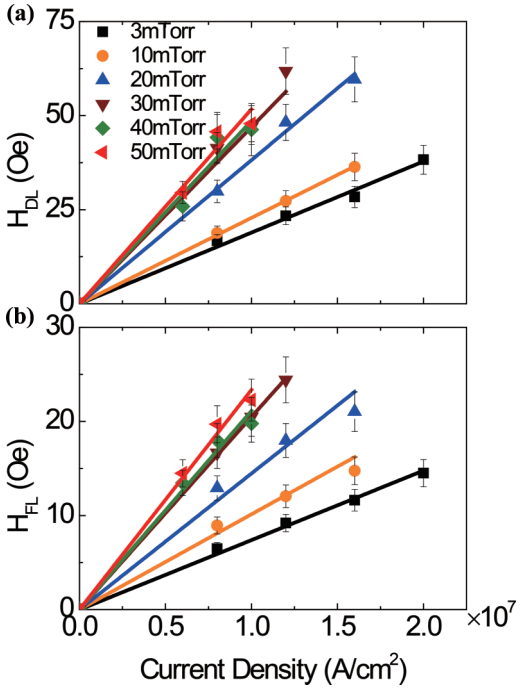

FIG. 3. Effective field as a function of current density for samples with various Pt deposition pressures. (a) Dampinglike effective field, H_{DL}. (b) Fieldlike effective field, H_{FL}.

toward the in-plane field direction. The larger $V_{1\omega}$ at zero magnetic field for samples with Pt grown at higher pressures is attributed to a higher Pt resistivity since more current flows through the ferromagnetic Co layer while M_s remains the same for all samples [Fig. 1(d)] [27]. Note that $V_{1\omega}$ has the same value for both in-plane H_x and H_y magnetic field. On the other hand, $V_{2\omega}$, which is related to SOT-induced effective fields, depends on whether the magnetic field direction is parallel (H_x) or transverse (H_y) to the current direction. Figures 2(c) and 2(d) show $V_{2\omega}$ as a function of H_x and H_y, representing the two orthogonal components of the SOT, i.e., the dampinglike (DL) and fieldlike (FL) SOT components, respectively [24,28–30]. An overall increase in the slope of $V_{2\omega}$ was observed with increasing Pt deposition pressure, indicating an enhancement in the effective fields induced by both dampinglike and fieldlike torques. The SOT-induced effective fields for a small polar angle can be extracted using $H_{DL(FL)} = -2[(\partial V_{2\omega,x(y)}/\partial H_{x(y)})]/(\partial^2 V_{\omega,x(y)}/\partial H^2_{x(y)})$ [31]. Figures 3(a) and 3(b) show H_{DL} (i.e., an effective field corresponding to dampinglike SOT) and H_{FL} (i.e., an effective field corresponding to fieldlike SOT), respectively, obtained at various current densities for each sample grown under different pressure. Note that the resistivity of Ta and Co is 541 $\mu\Omega$ cm and 67.8 $\mu\Omega$ cm, respectively, and the current density is calculated assuming the current flowing only through the Pt/Co layers. A linear increase in both H_{DL} and H_{FL} with current density is observed, as well as an increase in the slope for samples with larger Pt resistivities. The H_{DL} vs current density in Fig. 3(a) allows us to extract the effective spin-Hall angle as $\theta_{SH,eff} = 2eM_s t_F H_{DL}/\hbar|j_e|$ [32], where e is the electron charge, $\hbar$ is the reduced Planck constant, j_e is the charge-current density, and t_F is the ferromagnet thickness. It turns out that $\theta_{SH,eff}$ increases about three times while the resistivity of Pt layer increases by a factor of 1.6 [see Fig. 2(e)]. This is consistent with previous works [19] reporting that the spin-Hall angle of a Pt single layer increases proportionally to its resistivity using a lateral spin value in nonlocal geometry. This result however differs from our result in which the spin transport in Pt is influenced by an interfaced FM Co. Proximity effects in Pt may also contribute to the variation of effective θ_{SH} [33]. However, there is no significant variation in the saturation magnetization between the samples [Fig. 1(d)], suggesting that the proximity-induced magnetic moment in Pt does not change with Ar deposition pressure. Thus, a change in the proximity effect due to the Ar pressure is not the main origin of the enhanced effective spin-Hall angle.

In order to confirm the increase in $\theta_{SH,eff}$ we performed SOT-induced switching experiments, where the magnetization direction was monitored by measuring the anomalous Hall resistance (R_H) with a sensing current of 100 μA while sweeping a pulsed driving current up to ±25 mA with step size of 0.5 mA. The results, shown in Fig. 4(a), demonstrate deterministic SOT-induced switching of perpendicular magnetization. It was observed that a positive (negative) current favors magnetization alignment along the $-z$ ($+z$) direction

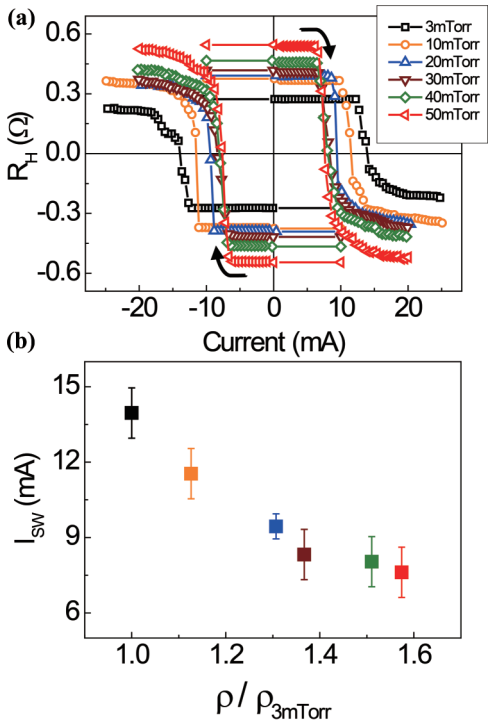

FIG. 4. Magnetization switching. (a) SOT-induced magnetization switching for Pt/Co/AlO_x stack with various Pt deposition pressures. (b) Switching current (I_{sw}) as a function of Pt resistivity normalized by that for 3 mTorr ($\rho/\rho_{3\,\mathrm{mTorr}}$).

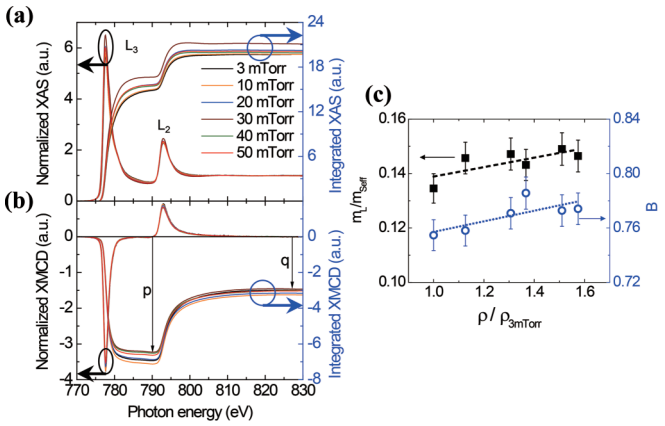

FIG. 5. XAS and XMCD measurements and analysis for samples with Pt layers grown under varying pressure conditions. (a) XAS at the Co $L_{2,3}$ edge. Spectra have been normalized to the averaged XAS signal at the high-energy side, after background subtraction. Integrated intensities of the spectra are also shown, from which the branching ratio B can be obtained. (b) Corresponding XMCD spectra, together with their integrated intensities. The vertical arrows indicate the values of p and q for application in the magneto-optical sum rules. (c) $m_L/m_{S,\mathrm{eff}}$ ratio (left axis) and B (right axis) for all samples obtained from the XAS and XMCD spectra at the Co $L_{2,3}$ edges. Dashed lines are guides to the eye.

under a positive in-plane magnetic field of 10 mT, which coincides with a positive spin-Hall angle of the Pt layer [3,8,9]. Moreover, as the Pt deposition pressure and thereby the Pt resistivity increase, the switching current I_{sw} decreases [Fig. 4(b)]. The decrease in switching current, or enhancement in the switching efficiency, is in good agreement with the enhancement in the effective spin-Hall angle obtained by the harmonic lock-in technique.

We have shown that the effective spin-Hall angle of Pt increases with the Pt resistivity, consistent with the theoretical prediction [20]. In the same study [20] it was also predicted that the interface contribution to the spin-Hall effect is about 26 times larger than that of the bulk. This implies that the enhancement factor of the SOT would be larger than the enhancement factor of the resistivity since more current flows near the Co/Pt interface as the Pt resistivity increases. This implication is in accord with our experimental observation: the enhancement factor of the spin-Hall angle is 3.0 while the enhancement factor of the Pt resistivity is 1.6. Moreover, our results of a non-negligible fieldlike torque (H_{FL}), which is about half the dampinglike torque (H_{DL}), and an increase in H_{FL} with the Pt resistivity (Fig. 3) support our claim about the interfacial contribution enhancement with Pt resistivity since the fieldlike torque is often described by the interfacial spin-orbit coupling effect [34]. We note that such relatively large $H_{\mathrm{FL}}/H_{\mathrm{DL}}$ is hard to explain exclusively by the bulk spin-Hall effect since the $H_{\mathrm{FL}}/H_{\mathrm{DL}}$ in the bulk spin-Hall effect mechanism is determined by $\mathrm{Im}(G_{\uparrow\downarrow})/\mathrm{Re}(G_{\uparrow\downarrow})$, which is known to be small, where $\mathrm{Re}(G_{\uparrow\downarrow})$ and $\mathrm{Im}(G_{\uparrow\downarrow})$ are, respectively, the real and imaginary parts of the spin-mixing conductance $G_{\uparrow\downarrow}$ at the FM/HM interface. In order to check the applicability of this argument against our results, we need to experimentally address such an interface contribution, which is related to the spin-orbit coupling-induced band splitting originating from the inversion-symmetry breaking at the interface. A recent *ab initio* study [35] found that the spin splitting originates from orbital hybridization which is associated with the charge transfer between the d orbitals in FM and HM. The orbital hybridization also results in an enhancement of the orbital-angular momentum; thus the interfacial SOT contribution is closely related to the orbital moment through spin-orbit coupling-induced band splitting.

We performed XAS and XMCD measurements to verify whether the interface spin-orbit coupling as a function of Pt resistivity gives a significant contribution to the $\theta_{\mathrm{SH,eff}}$ in our samples. The XAS and XMCD spectra for the Pt(5 nm)/Co(0.8 nm)/AlO_x(1.8 nm) samples are shown in Figs. 5(a) and 5(b), together with their integrated intensities. These results allow us to obtain two quantities associated with the spin-orbit coupling of the Co atoms, namely the branching ratio B [36] and the orbital-to-spin magnetic moment ratio $m_L/m_{S,\mathrm{eff}}$ [37], where m_L and $m_{S,\mathrm{eff}}$ are the orbital moment and effective spin moment in the measured sample geometry. B is defined as the fraction of the total XAS intensity I in the L_3 edge, i.e., $B = I(L_3)/[I(L_3) + I(L_2)]$ and theoretically $B = B_0 + (\langle \ell \cdot s \rangle / n_h)$ [36], where B_0 is the branching ratio value without spin-orbit interaction (here considered to be a constant), l (s) is orbital (spin) angular momentum, and n_h is the number of d holes, so that $(B - B_0)$ is proportional to the ground-state expectation value of the angular part of the spin-orbit interaction $\ell \cdot s$ per Co $3d$ hole. Therefore, B provides a direct measure of the spin-orbit interaction in the local electronic structure of Co in the samples. The

orbital to spin moment ratio, on the other hand, is obtained by applying the magneto-optical sum rules to the XMCD signal as $m_L/m_{S,\mathrm{eff}} = 2q/(9p - 6q)$ [38–40], where p and q are the integrated XMCD intensities for the L_3 and $L_3 + L_2$ edges, respectively [see Fig. 5(b)]. We note that the $m_L/m_{S,\mathrm{eff}}$ ratio evaluates the interfacial spin-orbit interaction in FM/HM structures [41,42]. The obtained values of B and $m_L/m_{S,\mathrm{eff}}$ for all samples are plotted in Fig. 5(c), where both quantities show a gradual increase with Pt resistivity. This indicates that the spin-orbit interaction of the Co indeed increases with the resistivity of the Pt layer. Therefore, our result is in line with the theoretical prediction of Wang *et al.* [20], which emphasizes the important role of interfacial spin-orbit interaction that contributes to the increase in the effective spin-Hall angle. This is controlled using a material's parameter of HM, namely the resistivity in our study. Moreover, we should note that the increase in surface roughness of the Pt layer with Ar pressure (Table I) can also contribute to the enhanced spin-orbit torque as it was reported [43] that the surface roughness in ultrathin films can enhance the spin-Hall effect due to surface scattering through the side-jump scattering mechanism.

IV. CONCLUSION

We studied the effect of Pt resistivity on the SOT in $\mathrm{Pt/Co/AlO}_x$ where the Pt resistivity was controlled by varying the Ar deposition pressure. It was found that the SOT as well as the effective spin-Hall angle obtained using harmonic lock-in techniques is about 3 times enhanced, while the Pt resistivity increases only 1.6 times. This result provides an answer to our original question: the SOT strength increases indeed with the HM resistivity. Interestingly, our result is in agreement with the theoretical prediction of Wang *et al.* [20], who found an increased spin-Hall angle with HM resistivity and a dominant contribution of the FM/HM interface to SOT. This implies that the key factor to enhance the SOT would be the interface engineering combined with the layer design to concentrate more currents near the FM/HM interface. We expect our result to provide an efficient route for material engineering towards improved SOT-based spintronic devices.

ACKNOWLEDGMENTS

This work was supported by National Research Foundation of Korea funded by the Ministry of Science, ICT & Future Planning (Grants No. NRF-2015M3D1A1070465 and No. 2014R1A2A1A11051344). S.-Y.P. acknowledges financial support from the National Research Council of Science & Technology (NST) (Grant No. CAP-16-01-KIST). K.J.L. acknowledges the support from National Research Foundation of Korea funded by the Ministry of Science, ICT & Future Planning (Grant No. NRF-2017R1A2B2006119). We acknowledge the Diamond Light Source for beamtime on I10 under proposal SI-13410.

[1] S. A. Wolf, D. D. Awschalom, R. A. Buhrman, J. M. Daughton, S. von Molnar, M. L. Roukes, A. Y. Chtchelkanova, and D. M. Treger, Science **294**, 1488 (2001).
[2] I. Žutić, J. Fabian, and S. Das Sarma, Rev. Mod. Phys. **76**, 323 (2004).
[3] I. M. Miron, K. Garello, G. Gaudin, P.-J. Zermatten, M. V. Costache, S. Auffret, S. Bandiera, B. Rodmacq, A. Schuhl, and P. Gambardella, Nature (London) **476**, 189 (2011).
[4] L. Liu, C.-F. Pai, Y. Li, H. W. Tseng, D. C. Ralph, and R. A. Buhrman, Science **336**, 555 (2012).
[5] D. C. Ralph and M. D. Stiles, J. Magn. Magn. Mater. **320**, 1190 (2008).
[6] A. R. Mellnik, J. S. Lee, A. Richardella, J. L. Grab, P. J. Mintun, M. H. Fischer, A. Vaezi, A. Manchon, E.-A. Kim, N. Samarth, and D. C. Ralph, Nature (London) **511**, 449 (2014).
[7] Y. Fan, P. Upadhyaya, X. Kou, M. Lang, S. Takei, Z. Wang, J. Tang, L. He, L.-T. Chang, M. Montazeri, G. Yu, W. Jiang, T. Nie, R. N. Schwartz, Y. Tserkovnyak, and K. L. Wang, Nat. Mater. **13**, 699 (2014).
[8] Y. Wang, P. Deorani, X. Qiu, J. H. Kwon, and H. Yang, Appl. Phys. Lett. **105**, 152412 (2014).
[9] H. L. Wang, C. H. Du, Y. Pu, R. Adur, P. C. Hammel, and F. Y. Yang, Phys. Rev. Lett. **112**, 197201 (2014).
[10] C.-F. Pai, L. Liu, Y. Li, H. W. Tseng, D. C. Ralph, and R. A. Buhrman, Appl. Phys. Lett. **101**, 122404 (2012).
[11] B. Gu, I. Sugai, T. Ziman, G. Y. Guo, N. Nagaosa, T. Seki, K. Takanashi, and S. Maekawa, Phys. Rev. Lett. **105**, 216401 (2010).
[12] Y. Niimi, M. Morota, D. H. Wei, C. Deranlot, M. Basletic, A. Hamzic, A. Fert, and Y. Otani, Phys. Rev. Lett. **106**, 126601 (2011).
[13] Y. Niimi, Y. Kawanishi, D. H. Wei, C. Deranlot, H. X. Yang, M. Chshiev, T. Valet, A. Fert, and Y. Otani, Phys. Rev. Lett. **109**, 156602 (2012).
[14] S. Woo, M. Mann, A. J. Tan, L. Caretta, and G. S. D. Beach, Appl. Phys. Lett. **105**, 212404 (2014).
[15] S. Cho, S. C. Baek, K.-D. Lee, Y. Jo, and B.-G. Park, Sci. Rep. **5**, 14668 (2015).
[16] K.-U. Demasius, T. Phung, W. Zhang, B. P. Hughes, S.-H. Yang, A. Kellock, W. Han, A. Pushp, and S. S. P. Parkin, Nat. Commun. **7**, 10644 (2016).
[17] A. Hoffmann, IEEE Trans. Magn. **49**, 5172 (2013).
[18] T. Tanaka, H. Kontani, M. Naito, T. Naito, D. S. Hirashima, K. Yamada, and J. Inoue, Phys. Rev. B **77**, 165117 (2008).
[19] E. Sagasta, Y. Omori, M. Isasa, M. Gradhand, L. E. Hueso, Y. Niimi, Y. C. Otani, and F. Casanova, Phys. Rev. B **94**, 060412(R) (2016).
[20] L. Wang, R. J. H. Wesselink, Y. Liu, Z. Yuan, K. Xia, and P. J. Kelly, Phys. Rev. Lett. **116**, 196602 (2016).
[21] U. H. Pi, K. W. Kim, J. Y. Bae, S. C. Lee, Y. J. Cho, K. S. Kim, and S. Seo, Appl. Phys. Lett. **97**, 162507 (2010).
[22] K. Garello, I. M. Miron, C. O. Avci, F. Freimuth, Y. Mokrousov, S. Blügel, S. Auffret, O. Boulle, G. Gaudin, and P. Gambardella, Nat. Nanotechnol. **8**, 587 (2013).
[23] J. Kim, J. Sinha, M. Hayashi, M. Yamanouchi, S. Fukami, T. Suzuki, S. Mitani, and H. Ohno, Nat. Mater. **12**, 240 (2013).

[24] L. Liu, O. J. Lee, T. J. Gudmundsen, D. C. Ralph, and R. A. Buhrman, Phys. Rev. Lett. **109**, 096602 (2012).
[25] Y.-W. Oh, S. Chris Baek, Y. M. Kim, H. Y. Lee, K.-D. Lee, C.-G. Yang, E.-S. Park, K.-S. Lee, K.-W. Kim, G. Go, J.-R. Jeong, B.-C. Min, H.-W. Lee, K.-J. Lee, and B.-G. Park, Nat. Nanotechnol. **11**, 878 (2016).
[26] R. Messier, A. P. Giri, and R. A. Roy, J. Vac. Sci. Technol. A **2**, 500 (1984).
[27] N. Nagaosa, J. Sinova, S. Onoda, A. H. MacDonald, and N. P. Ong, Rev. Mod. Phys. **82**, 1539 (2010).
[28] A. Manchon and S. Zhang, Phys. Rev. B **79**, 094422 (2009).
[29] S. Emori, U. Bauer, S.-M. Ahn, E. Martinez, and G. S. D. Beach, Nat. Mater. **12**, 611 (2013).
[30] I. M. Miron, G. Gaudin, S. Auffret, B. Rodmacq, A. Schuhl, S. Pizzini, J. Vogel, and P. Gambardella, Nat. Mater. **9**, 230 (2010).
[31] M. Hayashi, J. Kim, M. Yamanouchi, and H. Ohno, Phys. Rev. B **89**, 144425 (2014).
[32] A. V. Khvalkovskiy, V. Cros, D. Apalkov, V. Nikitin, M. Krounbi, K. A. Zvezdin, A. Anane, J. Grollier, and A. Fert, Phys. Rev. B **87**, 020402(R) (2013).
[33] W. Zhang, M. B. Jungfleisch, W. Jiang, Y. Liu, J. E. Pearson, S. G. E. te Velthuis, A. Hoffmann, F. Freimuth, and Y. Mokrousov, Phys. Rev. B **91**, 115316 (2015).
[34] P. M. Haney, H.-W. Lee, K.-J. Lee, A. Manchon, and M. D. Stiles, Phys. Rev. B **87**, 174411 (2013).
[35] S. Grytsyuk, A. Belabbes, P. M. Haney, H.-W. Lee, K.-J. Lee, M. D. Stiles, U. Schwingenschlögl, and A. Manchon, Phys. Rev. B **93**, 174421 (2016).
[36] B. T. Thole and G. van der Laan, Phys. Rev. B **38**, 3158 (1988).
[37] Y. Wu, J. Stöhr, B. D. Hermsmeier, M. G. Samant, and D. Weller, Phys. Rev. Lett. **69**, 2307 (1992).
[38] B. T. Thole, P. Carra, F. Sette, and G. van der Laan, Phys. Rev. Lett. **68**, 1943 (1992).
[39] P. Carra, B. T. Thole, M. Altarelli, and X. Wang, Phys. Rev. Lett. **70**, 694 (1993).
[40] G. van der Laan and A. I. Figueroa, Coord. Chem. Rev. **277–278**, 95 (2014).
[41] C. Nistor, T. Balashov, J. J. Kavich, A. Lodi Rizzini, B. Ballesteros, G. Gaudin, S. Auffret, B. Rodmacq, S. S. Dhesi, and P. Gambardella, Phys. Rev. B **84**, 054464 (2011).
[42] X. Qiu, K. Narayanapillai, Y. Wu, P. Deorani, D.-H. Yang, W.-S. Noh, J.-H. Park, K.-J. Lee, H.-W. Lee, and H. Yang, Nat. Nanotechnol. **10**, 333 (2015).
[43] L. Zhou, V. L. Grigoryan, S. Maekawa, X. Wang, and J. Xiao, Phys. Rev. B **91**, 045407 (2015).